Numerical modelling and applications of laser-accelerated ion beams

E. Lefebvre [a,*], E. d'Humières [a,b], L. Gremillet [a], S. Fritzler [c], V. Malka [d]

[a] *Département de Physique Théorique et Appliquée, Commissariat à l'Energie Atomique, DAM/DIF, BP 12, 91680 Bruyères-le-Châtel, France*

[b] *National Terawatt Facility, MS-372, University of Nevada, Reno, Nevada 89557, USA*

[c] *Siemens Medical Solutions, Vacuum Technology, 91052 Erlangen, Germany*

[d] *Laboratoire dOptique Appliquée, ENSTA, UMR 7639 CNRS / Ecole Polytechnique, 91761 Palaiseau, France*

Abstract

We use laser-plasma interaction and particle-transport codes to investigate ion acceleration when a short, intense laser pulse irradiates a thin solid foil, and to quantifiy the isotope yield that these ions can induce by nuclear reactions in secondary targets. Optimum acceleration, in terms of peak ion energy and secondary target activation, is obtained for ultra-low (sub-μm) target thickness.

Key words: Laser-plasma interaction, Ion acceleration, Particle-In-Cell simulation, Isotope production

1. Introduction

Ion acceleration with short-duration, high-intensity lasers is a subject of active research today in the laser-plasma community. Experiments using Terawatt and Petawatt-class laser facilities have observed well-collimated, energetic beams of protons accelerated away from the rear surface of a thin, solid target irradiated by intense ($I > 10^{18}$ W/cm^2) laser radiation [1]. The front target surface is first ionized by the low-intensity light pulse preceding the main, high-intensity pulse. Impinging radiation is then absorbed in this plasma, and electrons are accelerated to multi-MeV energies into the bulk of the target by the large electromagnetic fields (both incident and self-generated). A micrometer-thick solid target cannot significantly slow down this beam of relativistic electrons, and they rapidly reach the target back surface. As electrons exit into vacuum, a space-charge potential builds around the target, which finally reflects electrons back towards the target. This results in a cloud of energetic electrons orbiting around the positively-charged target, and setting up a strong electrostatic field at its front and rear surfaces. This field pulls positively-charged ions out of the target [2], among which protons are preferentially accelerated owing to their larger charge-to-mass ratio. Protons have been measured from a variety of targets, regardless of their material, as they originate from hydrogen-rich pollution adsorbed or deposited on the rear surface. Surface cleaning prior to the laser shot leads to their suppression and acceleration of heavier ion species [3].

Due to their short duration, high energy, and low emittance, these ion beams are recognized as potentially interesting for a number of applications, including rapid heating of solid matter [4], radiography of dense imploding material [5] or electrostatic fields in a plasma [6], isotope production [7,8] or cancer treatment [9,10]. Section 2 of this paper gives a rapid overview of the numerical tools we use to model ion acceleration and some of the above-mentioned applications.

* Corresponding author.
Email address: erik.lefebvre@cea.fr (E. Lefebvre).

Numerical simulation can play an important role in understanding and optimizing these ion sources, as much of the underlying physics occurs on time and space scales too short to be experimentaly resolved. Simplified, more or less *ad hoc* models of ion acceleration have been proposed [11], linking the peak proton energy to laser intensity and duration, and to target thickness. Together with experiments [12], they indicate that thinner target will accelerate protons to higher energy. This is due to the fact that in a thinner target, hot electrons are confined to a smaller volume, and the resulting higher hot electron density generates a larger accelerating field for the ions. This trend is also supported by simulations [13], which reveal additional phenomena at very small, sub-μm thicknesses. In the third section of this article, we use numerical simulations to delve further into this dependence of proton energy on target thickness, and establish the conditions allowing ion acceleration to the highest energies. In section 4, we study the potential of these laser-based ion sources for medical isotope production and show that significantly higher isotope yields can also be obtained by working with small target thicknesses.

2. Numerical models

Acceleration of ions by electrostatic fields and subsequent ion propagation and slowing down in a secondary target require two different physical models. Laser-plasma interaction and ion acceleration are essentially collisionless phenomena, governed by long-range fields, and where the full set of Maxwell equations must be solved to account for laser propagation, absorption, and the generation of self-consistent fields. A kinetic description of the plasma response is needed as we are chiefly interested at this point in the characteristics of relativistic electrons accelerated from the laser focal spot. In this article, we use the massively parallel, relativistic Particle-In-Cell code CALDER in 2D geometry to solve the Vlasov-Maxwell system. Consistently with the general physical picture given above, we assume in these simulations that the plasma is initially fully ionized, hence consisting of electrons and protons only, and we neglect collisions between particles.

On the contrary, ion propagation, slowing down, and ion-induced nuclear reactions in a secondary target are essentially collisional processes, in which laser and collective electromagnetic fields play no role. These phenomena are modelled with a Monte Carlo method using a continuous slowing down approximation for the ions and Ziegler formula [14] for the stopping power in various cold materials. Tabulated nuclear reaction cross sections found in well-known databases [15] are used to compute isotope production as the ions slow down in the target.

3. Ion acceleration

The first setup we consider [13] is a $10n_c$ (n_c denotes the critical density, 1.1×10^{21} cm^{-3} for a 1 μm wavelength laser) hydrogen target with thickness ranging from 0.05 to 6 μm, irradiated by a 36 fs duration, 1 μm wavelength laser pulse focused to 10^{20} W/cm^2 under normal incidence. Four snapshots of the ion density during the calculation are presented in Figure 1, for a target thickness of 0.73 μm. The first panel illustrates the inital target position, before the laser pulse, incident from the left, has reached its surface. At the time of the second snapshot, the pulse has already interacted with the target and heated a fraction of the plasma electrons. These electrons then drive ion expansion from the target front and back surfaces, which proceeds in the next two panels. This illustrates how different the time scales for laser-plasma interaction and ion acceleration can be: the former is limited to the pulse duration (36 fs here), whereas the latter can take hundreds of femtoseconds. This puts particularly stringent requirements on energy conservation in these simulations, for which large numbers of particles per cells (up to 500) were used.

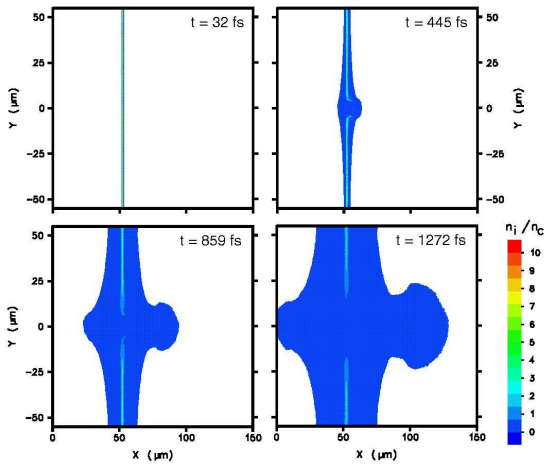

Fig. 1. Four snapshots of the ion density during and after interaction of a 10^{20} W/cm^2, 36 fs laser pulse with a $10n_c$, 0.73 μm-thick hydrogen target

The two ion blow-offs visible in Figure 1 correspond to large spreads in the energy distributions of these particles. 1.1 ps after the peak of the laser pulse has hit the target surface, the peak ion energy is measured in the simulation. It is always that of the right-most proton, located on the laser axis. This peak proton energy is plotted in Figure 2 as a function of target thickness. The non-monotonic trend of this curve can be explained as follows: at very low thickness, the laser pulse rapidly bores through the target, which has too little areal density (and hence current) to efficiently reflect the incoming light. Target density drops very rapidly and a large energy fraction is transmitted through the target, resulting in low laser coupling to the plasma and little ion acceleration. For large thickness, a gentle decrease with thickness is observed, consistent with experimental observations and attributed to the lower hot electron density in the space-charge sheath at the target rear surface. An interesting behaviour is observed in the intermediate thickness range, with a two-fold increase in peak ion energy [13]. This is attributed to relativistic plasma transparency [16], which enables light penetration and electron heating *inside* the target, thus providing a larger hot electron density to drive ion expansion. This mechanism also operates at smaller thicknesses, but in this case the target disassembles too early for the laser to be absorbed efficiently.

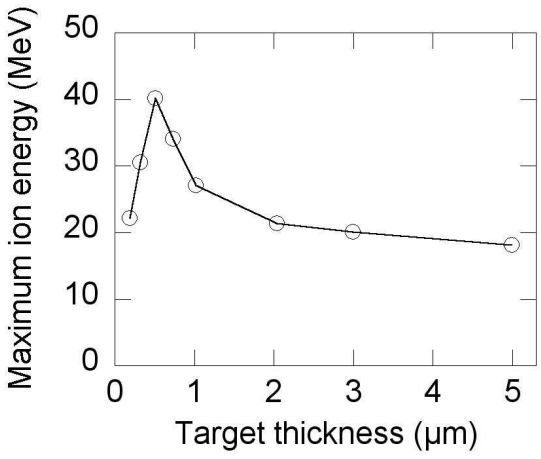

Fig. 2. Variations of peak proton energy with thickness of a $10n_c$ target. The normaly incident laser pulse has a 36 fs FWHM duration and a peak intensity of 10^{20} W/cm^2

Recent experiments [17,18] have tried to confirm this numerical prediction of improved ion acceleration for ultra-low thickness targets, but in [18], only a gentle energy increase with lower thickness is observed, and little transmission through the target is reported. Our initial simulations [13] and this experiment actually differ in many respects: oblique incidence, lower laser irradiance and a much higher initial target density were used in the experiment. This prompted us to perform additional simulations using the experimental parameters. The results, plotted in Figure 3, underline the dependence of ion acceleration on these parameters, and show good overall agreement with the results reported in [18], with little laser energy transmitted through the thin solid target and peak ion energies in the 5 MeV range, weakly dependent on thickness. Transition to a 'transparent' acceleration regime is only apparent below 20 nm, a thickness for which prepulse perturbation of the acceleration process is apparent in the results of [18].

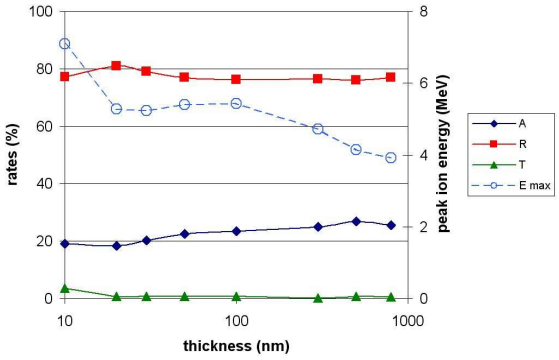

Fig. 3. Variations of maximum proton energy and laser absorption (A), reflection (R) and transmission (R) rates with thickness of a $150n_c$ target. The 0.8 μm-wavelength laser pulse is incident at 30° from target normal, has a 30 fs FWHM duration and a peak intensity of 10^{19} W/cm^2

4. Isotope production

Positron Emission Tomography (PET) is a medical imaging diagnostic for which positron-emitting isotopes such as ^{11}C and ^{18}F are needed. These isotopes are usually produced by irradiating targets containing, e.g., ^{11}B or ^{18}O nuclei with a high-intensity proton beam. Lasers are considered as an alternative for acceleration of this proton beam [19], with significants advantages (size, weight, versatility) over conventional sources such as cyclotrons.

Starting from the proton distributions obtained in the PIC simulations of Section 3, we used a particle transport and nuclear reaction code to compute

proton propagation though solid boron foils, and the ^{11}C activity induced by ^{11}B$(p,n)^{11}$C reaction during this propagation. The results are plotted in Figure 4 as a function of the proton-producing target thickness, and show the same variation with thickness as that observed in Figure 2 for the peak ion energy. This underlines the interest of the 'transparent' acceleration regime for applications. The order of magnitude of the resulting activity is a few kBq, much too small to have any medical interest as such. Still, significant activities are readily obtained if one takes advantage of a 1 kHz laser repetition rate: accounting for isotope decay during irradiation, one then computes an activity of 9.7 GBq after irradiation for one hour. This amount of isotope would be enough for preparation of several diagnostics samples. Activity scales roughly linearly with repetition rate, but simulations indicate that scaling with incident laser intensity is faster than linearly. Larger isotope production can hence be expected from laser facilities that would deliver more intense laser pulses, even if at a lower repetition rate [20].

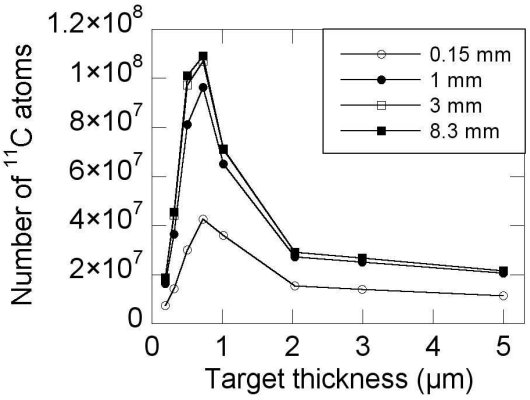

Fig. 4. Number of ^{11}C atoms produced by ^{11}B$(p,n)^{11}$C reaction in a solid boron catcher of variable thickness, as a function of the proton-producing target thickness

5. Conclusions

Multi-dimensional, fully relativistic, kinetic Particle-In-Cell codes are key numerical tools to explore high-intensity laser-plasma interaction. Recent studies devoted to ion acceleration in this high-field regime (I $> 10^{18}$ W/cm^2) have helped understand the sensitivity of this mechanism to target density and thickness, and laser intensity and duration. An improved acceleration regime relying on relativistic plasma transparency has been identified, leading to ion acceleration to higher energy and larger isotope yields when the ion beam is used to induce nuclear reactions in a secondary target. Significant amounts of medical isotopes could be produced with this new ion source, but the economic viability of this scheme will ultimately depend on the cost and reliability of high-intensity, energetic, kHz-repetition rate lasers that are yet to come.

Acknowledgements

E. L. acknowledges interesting and encouraging discussions with T. Ceccotti, J. Fuchs, A. Lévy, D. Neely, and Ph. Martin.

References

[1] M. Borghesi et al., Fusion Science Tech. 49 (2006) 412, and references therein.

[2] P. Mora, Phys. Rev. Lett. 90 (2003) 185002.

[3] M. Hegelich et al., Phys. Rev. Lett. 89 (2002) 085002.

[4] P. K. Patel et al., Phys. Rev. Lett. 92 (2003) 125004.

[5] A. J. Mackinnon et al., Phys. Rev. Lett. 97 (2006) 045001.

[6] M. Borghesi et al., Phys. Rev. Lett. 92 (2004) 055003.

[7] K. W. D. Ledingham, P. McKenna, and R. P. Singhal, Science 300 (2003) 1107.

[8] E. Lefebvre et al., to appear in J. Appl. Phys. 100 (2006).

[9] S. V. Bulanov and V. S. Khoroshkov, Plasma Physics Reports 28 (2002) 453.

[10] V. Malka et al., Med. Phys. 31 (2004) 1587.

[11] J. Fuchs et al., Nat. Phys. 2 (2006) 48.

[12] A. J. Mackinnon et al., Phys. Rev. Lett. 88 (2002) 215006.

[13] E. d'Humières, E. Lefebvre, L. Gremillet, and V. Malka Phys. Plasmas 12 (2005) 062704.

[14] J. F.Ziegler, J. Appl. Phys. 85 (1999) 1249.

[15] `http://www.nndc.bnl.gov/index.jsp`.

[16] E. Lefebvre and G. Bonnaud, Phys. Rev. Lett. 74 (1994) 2002.

[17] J. Fuchs et al., J. Phys. IV 133 (2006) 1151.

[18] D. Neely et al., Appl. Phy. Lett. 89 (2006) 021502.

[19] K. W. D. Ledingham et al., J. Phys. D: Appl. Phys. 37 (2004) 2341.

[20] E. Lefebvre et al., in preparation.